Mechanical subsystems integration and structural analysis for the autonomous underwater explorer

Jose Villa[1]*, Arttu Heininen[1]*, Soheil Zavari [1], Tuomas Salomaa[1],
Olli Usenius[1], Jouko Laitinen[1], Jussi Aaltonen[1] and Kari T. Koskinen[1]

***Abstract*— The aim of this study is to analyse the modular mechanical design and integration of all three low-level modules in UX-1 (pendulum, ballast system and propulsion unit). The components of the perception and navigation systems have position and orientation requirements that dictate the shape of the hull. A structural strength analysis using Finite Element Method (FEM) was made to study the hull strength during deep dives. The results are presented here, which indicates that the hull endures pressures related to deep dives. Also for validation, strain gauge locations were defined.**

I. INTRODUCTION

In recent years, research effort on autonomous vehicles has rapidly increased. Environments, where these vehicles are used, are more difficult than in the past. One of these are abandoned flooded mines, where tight corridors, lack of outside signal receiving, and deep shafts form a challenging environment. To design and develop an autonomous underwater vehicle for these harsh conditions, an EU-funded project UNEXMIN was launched. The aim of the project is to enable autonomous exploration and mapping of Europe's abandoned flooded mines. UX-1 is the robot used in UNEXMIN project for the Robotic Explorer platform. One key research challenge in this project is miniaturization of deep sea technology, as all components must fit inside a sphere of 600 mm diameter.

The UX-1 robot system layout contains several subsystems that can be combined into three groups: 1) perception system, which gathers data from the environment and forms situational awareness, 2) low-level control subsystems that enables the movement in all six degrees of freedom (DoF), and 3) geoscientific equipment, which is used to obtain and measure geoscientific data [3]. All these three groups require certain position and orientation inside the UX-1, making the integration a challenging process.

One of the main functions of the hull of a submersible vehicle is to protect the equipment within from water. This is achieved if the pressure hull can handle the loads that are stressing it [5]. With submersible vehicles, the dominant load is the surrounding water pressure. This pressure is directly proportional to the operating depth of the vehicle and increases by one bar for every ten meters. For vehicles that operate in shallow waters, waterproof hull is easy to design. As the water pressure is low, it does not limit the shape, or the materials used. However, the deeper the vehicle has to dive, the more limited the hull design is.

As mines are often deep, from tens of meters to even kilometers, UX-1 must be able to withstand high pressure. To handle hydrostatic pressure on a submerged body, it is well known that a spherical shape is best suitable. However, UX-1 has other design constrains also. Mine corridors are not wide, so the maximum size is limited, and perception and navigation equipment requires certain placement for them to operate correctly. These two constrains conflict with the spherical shape and a trade-off between these is required.

Research on spherical unmanned and autonomous underwater vehicles started in the early 1990s with the Omni-Directional Intelligent Navigator (ODIN). This robot provides 6 DoF with 8 thrusters, sonar and pressure sensor and inertial navigation system [6]. More recently platforms with a spherical hull has been used to develop vectored water-jet based propulsion system [7], [8], [9] and amphibious robots [10]. Also, spherical platforms with a pendulum [11] and a variable ballast tank [12], both of which are included in the UX-1 design, have been considered. However, these applications are limited to shallow waters as their hull cannot withstand high pressures. Therefore, a novel hull design is introduced.

In this work, subsystems integration in the spherical underwater vehicle UX-1 is studied following shape and size specifications and satisfying all the situational awareness and geoscientific instrumentation requirements. In addition, a structural analysis is done to validate the pressure hull design and to prove that the integration accomplishes the necessary requirements. Furthermore, the structural analysis results are used to define strain gauge locations for a pressure test.

II. SUBSYSTEMS INTEGRATION IN A SPHERICAL UNDERWATER VEHICLE

A. Description of UX-1 subsystems

All subsystems groups mentioned in Section I are necessary for the correct operation of the UX-1. However, there are certain components that need to be placed in a certain position and orientation to operate correctly. These components are included in the perception and low level control systems. Regarding the perception system components, the set of sensors under consideration is comprised of cameras, laser line projectors, M3 multibeam sonar, and a mechanical

[1]J. Villa, A. Heininen, S. Zavari, T. Salomaa, O. Usenius, J. Laitinen, J. Aaltonen and K. T. Koskinen are with Faculty of Engineering Science, Mechanical Engineering and Industrial systems, Tampere University of Technology (TUT), Tampere, Finland jose.villa, arttu.heininen, soheil.zavari, tuomas.salomaa, olli.usenius, jouko.laitinen, jussi.aaltonen, kari.t.koskinen@tut.fi

* These authors contributed equally to this work.

scanning sonar [4]. The mechanical subsystems consists of a propulsion unit, a pendulum mechanism and a ballast system [1], [2] and they are shown in the Fig. 1. Finally, there is the geoscientific equipment, such as water sampler unit, sub-bottom profiler and a set of PH-sensors, which are out of the scope of this paper as they do not have significant positioning restrictions.

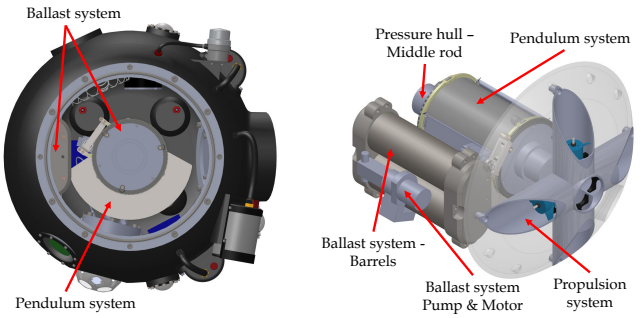

(a) (b)

Fig. 1. Control mechanisms integrated in the UX-1

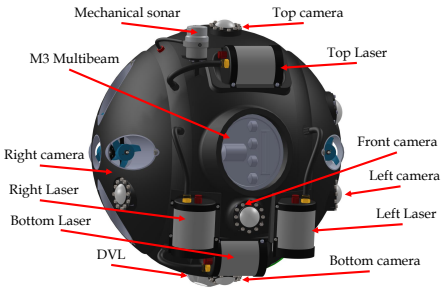

Fig. 2. Perception system components

B. Subsystems Integration

Perception system components and low-level control mechanisms need to be included in the integrated pressure hull design of the underwater explorer. The major constraint in the subsystem integration and therefore, in the pressure hull design, is the perception system. All necessary instrumentation for the perception system are shown in Fig. 2. Furthermore, Fig. 3 shows the axes of all sensor links, where the x, y, z axis are red, blue and green respectively. These axes are related to the required position and orientation of the perception system [4]. These requirements in position and orientation make the pressure hull design a challenging process due to the necessity of cases or pockets for every component which is in contact with water.

These cases mean that a perfect sphere cannot be used as a pressure hull. Moreover, majority of them are in front of the hull within close vicinity of each other as Fig. 4 shows. The pressure hull design is based on three individual parts made of aluminum: two lateral side hulls on each side of the robot and a central hull. The integration of these parts is based on a center beam that supports the lateral hulls. The center

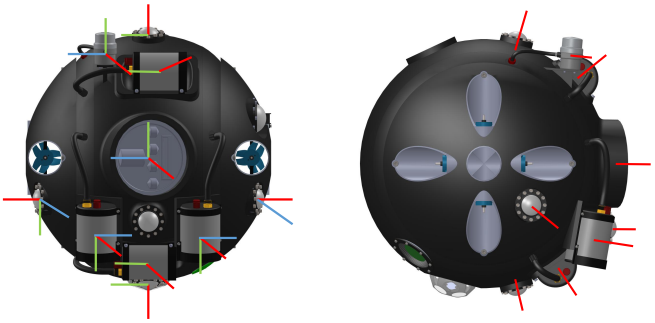

(a) Front view (b) Right view

Fig. 3. Perception system - Robot axes

beam is required as the lateral parts are flat, instead of a round shape, due to camera cases included in the perception system.

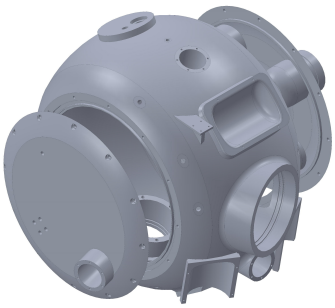

Fig. 4. Pressure hull design - Deployed view

The center beam is also a major part of the low level control subsystem. As the space inside the hull is strictly limited, a solution for this subsystem that requires as little space as possible, is required. Further, this solution cannot hinder the operation of the subsystem components. The solution for this is to use the center beam as a common component for the pendulum and ballast system, which are two of the major components of the low level control subsystem. According to that, pendulum and ballast systems use the center beam as a common component, as the schematic diagram of Fig. 5 shows. Furthermore, all of these mechanical subsystems have to be designed and integrated fulfilling perception system restrictions.

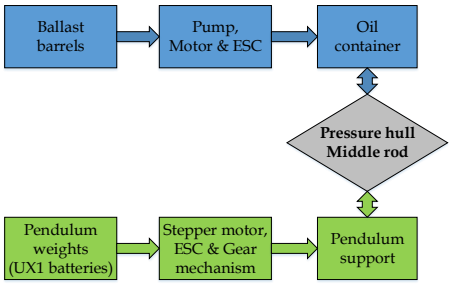

Fig. 5. Diagram subsystem integration with pressure hull

The propulsion system is formed by a total of 8 thrusters, located in two manifolds with four openings in both sides of the UX-1. The purpose of these manifolds is to enable the round shape in the lateral parts and to protect the thrusters from ropes, wires, and similar harmful objects that are present in mines. In addition to that, the manifolds increases the efficiency of the thrusters and enables use of the thrusters so, that it is possible to move robot in all three directions [1]. The manifolds are attached to the UX-1 lateral hulls. Furthermore, these manifolds are casted in a syntactic foam. This allows spherical shape on both lateral parts, and makes the design more rigid. Syntactic foam is required to achieve required buoyancy. Fig. 6 presents one of the manifolds in the propulsion system layout for the UX-1.

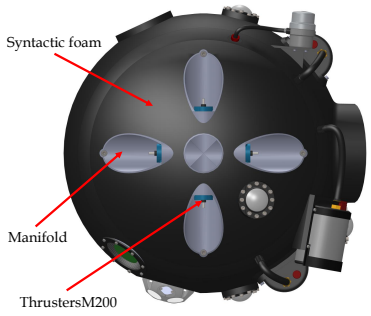

Fig. 6. Robot propulsion unit - Right side view

Regarding the position of the three low-level control, the center of the pendulum mechanism needs to be placed in the center of the UX-1. This is only possible if the pendulum mechanism is built around the center rod. Furthermore, it must be able to provide ± 90 degrees of pitch angle. This symmetry is only achieved, if the Center of Mass (CM) of UX-1 is located in the exact center of the spherical shape. Due to that, balancing must be made, i.e., all the components must be placed within UX-1 so that it does not rotate while in rest. For the balance test, the CM is obtained using computer model that has the components and equipment related to the three main subsystems. This result is used to place the rest of necessary components which do not have any position/orientation specification, such as power supply components (batteries) or computers for robots operation.

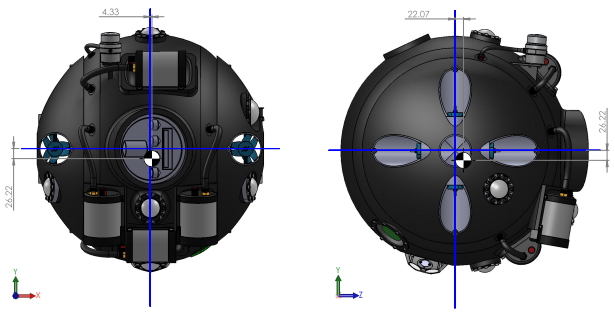

(a) Front view (b) Right view

Fig. 7. UX-1 Center of Mass according simulation

The previous results are obtained with all the UX-1 components installed. To compensate the difference between the CM and the origin (Table I), a series of extra weights are mounted in the UX-1 to obtain the CM as close as possible to the origin.

TABLE I
UX-1 CENTER OF MASS FROM ORIGIN

X $[mm]$	4.33
Y $[mm]$	26.22
Z $[mm]$	22.07

III. STRUCTURAL STRENGTH ANALYSIS

The loads that stress underwater vehicles during movement can be divided into two parts: hydrodynamic forces and surrounding water pressure. Hydrodynamic forces are proportional to the square of the velocity, water pressure, and the area of the submerged body. The surrounding water pressure increases along the depth of the vehicle. For fast-moving shallow water vehicles, the stress caused by hydrodynamic forces can be significant, i.e., larger or at least in the same magnitude than stress caused by water pressure. Instead, for slow-moving deep water vehicles the dominant load is water pressure. UX-1 belongs to the latter group. Also, there are forces related to actuators, e.g., thrusters and body forces like gravity and buoyancy, but these are small compared to pressure.

Pressure is a uniformly distributed loading, hence the best shape from the structural strength point of view is a sphere. However, the components related to the perception system discussed earlier, require a certain position and orientation. This means that the shape cannot be perfectly spherical, as there are components protruding from the hull, making the hull complex. The complexity means that a thorough structural strength analysis is required.

Using the Finite Element Method (FEM) [13], an analysis for the structural strength was conducted. As the design model had many fine features that are not required for the analysis, a simplified model was made. In the simplified model, the lateral parts and the central part form a single solid body. The final design has thrusters that are in manifolds, being immersed into the syntactic foam around the lateral parts. Both the syntactic foam and manifolds were removed from the simplified model. Also, the M3 multibeam sonar and DVL were removed.

A mesh based on the simplified model was generated for the strength analysis. The final mesh consists of 1.6 million 10-node quadratic tetrahedral elements, which are suitable for arbitrarily shaped solids. The mesh is shown in Fig. 8. The elements in the protruding components are refined to size of 4 mm, as these are the most interesting parts. The overall element size is 5 mm. After initial analysis, parts with high stress were refined to 2 mm.

After the mesh generation, the boundary conditions were set, i.e., water pressure compressing the outer surface. However, as the M3 multibeam and DVL are not present in the

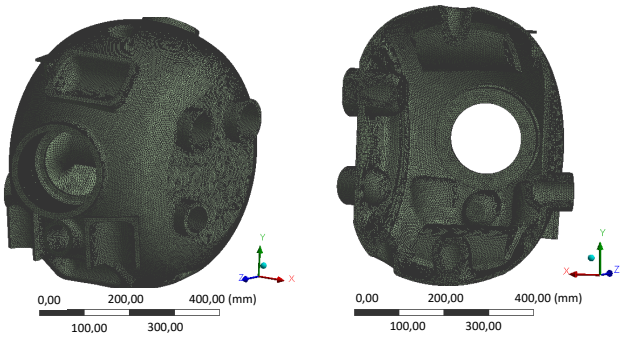

(a) (b)

Fig. 8. The mesh used in strength analysis outside (a) and inside (b)

model, the force affecting the support structures had to be separately calculated. Then, these forces were included in the boundary conditions. This was done also for the water sampler unit. If the calculated forces are not accurate, there will be resultant force, which accelerates the whole model, which is unrealistic. One of the calculated forces pushes the multibeam support structure inside UX-1, which is shown in Fig. 9 along other boundary conditions.

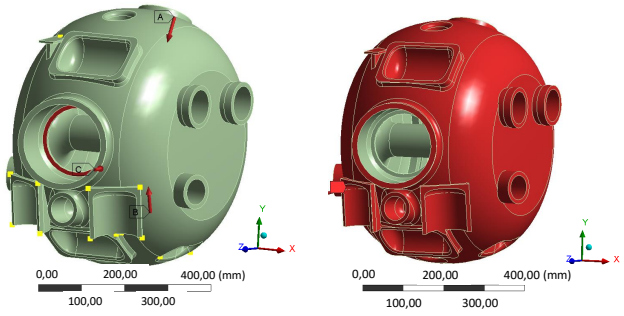

(a) (b)

Fig. 9. The boundary conditions: Forces (a) and Pressure (b)

The hull is equipped with all necessary instrumentation, which decreases the available air volume for buoyancy generation. However, UX-1 buoyancy must be neutral for energy saving. This limits the available materials that can be used in the hull. High strength steel would endure high stresses but it is too heavy. Also, there are cost restriction because of the complex shape of the casting, so special materials like titanium cannot be used. Due to these restrictions related to the buoyancy and cost of the UX-1, the material used for the pressure hull has to be light avoiding unnecessary weight in the structural components. Therefore, an aluminum alloy is used for the pressure hull, pressure cases and mounting pockets. Due to the complexity of the central part, it is manufactured by aluminum pouring casting method (Alloy AS7G06). The lateral parts are made by 5-axis machining as a monobloc (Alloy AW 7021). These alloys are high strength aluminum alloys and provides high enough strength for this application.

Finally, the structural response on the loading was calculated using different water pressures. The results shown here are from case, where the pressure was 30 bar. Fig. 10 shows the inverse of the safety factor inside and outside UX-1 with the minimum and maximum marked with a label. The deformation that shows in the figure is greatly exaggerated. The safety factor is calculated using equivalent von Mises stress, which is suitable for ductile materials, and this is compared to the yield stress of the material. The von Mises stress is:

$$\sigma_v = \sqrt{\frac{1}{2}(\sigma_1 - \sigma_2)^2 + (\sigma_2 - \sigma_3)^2 + (\sigma_3 - \sigma_1)^2}, \quad (1)$$

where σ_1, σ_2, σ_3 are principal stresses, and the safety factor is:

$$N = \frac{\sigma_y}{\sigma_v}, \quad (2)$$

where σ_y is the yield stress. The minimum value for safety factor is 1.31. In addition, the location of the highest strength is next to the lateral hull. As the simplified model is a single body, the connection between the central and lateral parts is almost rigid, whereas in reality, the lateral parts are connected to the central part with bolts allowing small deformation that relieves stress. On average, the safety factor is two or more.

As the project advances and consecutive deep dives are conducted, the hull is slowly fatigued. These consecutive dives equate to cyclic loading with low frequency but high amplitude. This means that even if the hull handles the loading of a single mission, it will eventually fail because of fatigue. The raw casting used to manufacture the central part is bound to have defects leading to local stress concentrations or microcracks [14]. These defects lead to larger cracks through what is called crack propagation. When one of these cracks becomes large enough the hull is compromised and will leak. Therefore, a fatigue life analysis must eventually be made before UX-1 is commissioned for full scale commercial operations.

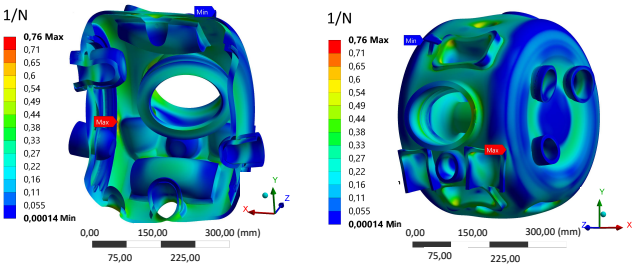

(a) (b)

Fig. 10. Inverse safety factor of UX-1 inside (a) and outside (b)

A pressure test is needed to validate the simulation results. The hull will be sealed and put into a pressure chamber that is filled with water. Then, the pressure inside the chamber is raised. Inside UX-1 there will be strain gauges that are connected to data logger through amplifiers. The schematic diagram of the strain measurement setup is shown in Fig. 11.

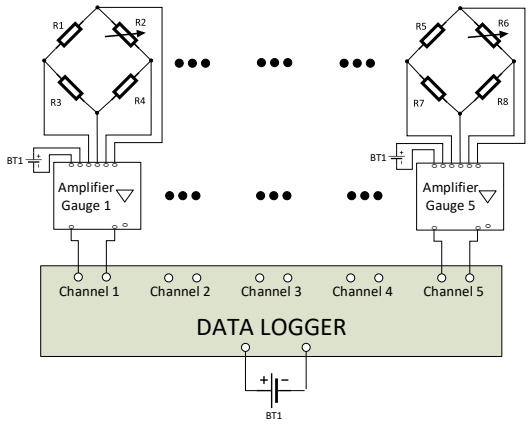

Fig. 11. Schematics of the strain measurement setup

The measurement setup consists of five full Wheatstone-bridges that are connected to amplifiers. One of the four resistors in a bridge is a strain gauge, and the other three are common resistors. Four of the strain gauges is connected to UX-1 hull and one is reserved for temperature effect elimination, as the strain gauges have different thermal expansion coefficient than UX-1. According to Hooke's law, the stress is related to strain through:

$$\sigma = E\epsilon, \tag{3}$$

where E is the elastic modulus of the material, and ϵ is strain. This constitutive equation can be used to solve stress from the measured strain, and both of these can be compared to simulation results to validate the simulation model.

The strain gauge locations are defined from the FEM simulation. Locations must be chosen so that there are no high strain gradients around the gauge. The strain gauge measures average strain under it, and high gradients makes the measurement unreliable. The strain is defined by engineering strain:

$$\epsilon = \frac{\Delta L}{L}, \tag{4}$$

where ΔL is the change in the strain gauge length and L is the original length. Conventional strain gauges are meant for measuring engineering strain, not large deformation, and maximum strain allowed is usually few percent. Therefore, in the chosen strain gauge location the strain cannot be large. The strain gauge resistance is directly proportional to strain, and the change in resistance of a strain gauge is:

$$\Delta R = K_s \epsilon R_s, \tag{5}$$

where K_s is gauge factor, which is usually around 2, ϵ is strain and R_s is the resistance of the strain gauge. The output voltage of a full Wheatstone-bridge is:

$$E_{Out} = \frac{(R_s + \Delta R)R_3 - R_2 R_4}{(R_s + \Delta R + R_2)(R_3 + R_4)} E_{in}, \tag{6}$$

where R_2, R_3, R_4 are resistors and E_{in} is the input voltage. The strain can be calculated from the output voltage. However, if the strain is small, so is the change in the resistance and the measured voltage, as can be seen from equations 5 and 6. [15]

The chosen locations for the four strain gauges are shown in Fig. 12. Locations of the strain gauges are marked with a blue label that has the corresponding strain. The first gauge is located on the M3 multibeam support structure, because the rectangular hole for the multibeam connectors weaken the support. The second one is located close to left vertical camera casing and left lateral hull, which is near the high stress location discussed earlier. Third strain gauge is on the left side of the support rod, as it should provide good reference value for the simulation model along with the final gauge in the aft of the hull. These locations should give a comprehensive and accurate strain behavior of the hull.

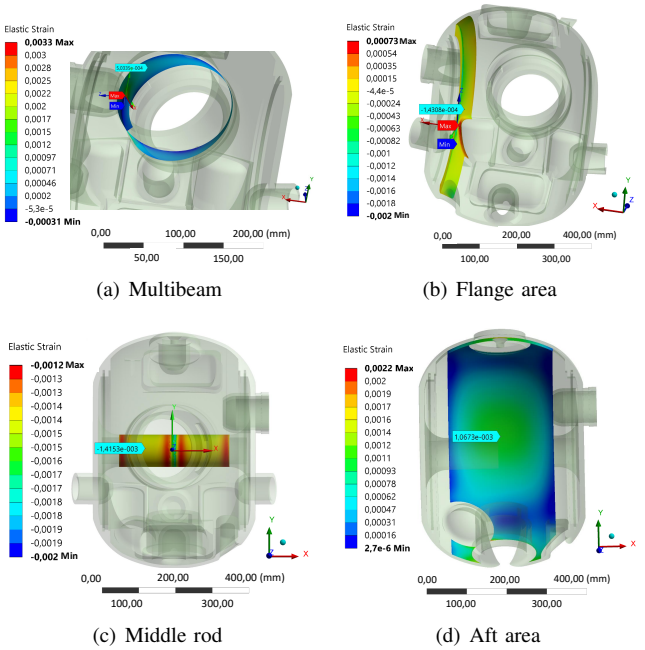

(a) Multibeam (b) Flange area

(c) Middle rod (d) Aft area

Fig. 12. Strain gauge positions and corresponding strain (Simulation)

Fig. 13 shows the installation of the strain gauges in the UX-1 pressure hull following the locations defined in Fig. 12. In addition to that, Fig. 14 shows the UX-1 pressure hull assembly with all necessary equipment installed for the pressure test.

IV. CONCLUSIONS

In conclusion, mechanical subsystems integration and pressure hull design need to be fulfill perception system requirements. These requirements mean that there is less space available inside of the UX-1 and impose the combination of components of the mechanical subsystems in single parts, as it is the middle rod of the pressure hull.

As UX-1 hull shape is not a perfect sphere, due to the protruding components, a thorough structural analysis was required. This analysis was made using finite element method with a simplified model. Based on the simplified model a mesh was created that had 1.6 million elements. The force acting on the M3 Multibeam and DVL support structure were

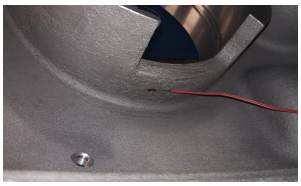

(a) Multibeam

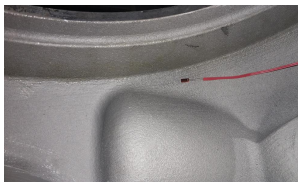

(b) Flange area

(c) Middle rod

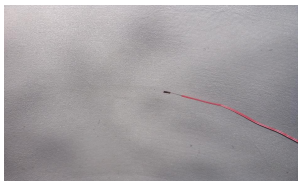

(d) Aft area

Fig. 13. Strain gauge positions (Test)

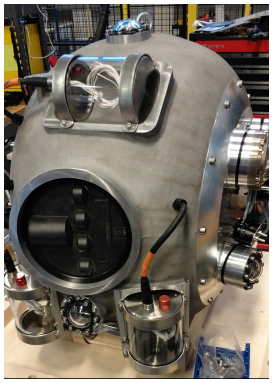

Fig. 14. UX-1 Complete pressure hull assembly

calculated. Boundary conditions included these forces and water pressure. The results show that the non-ideal spherical shape of the UX-1 is still valid for operations in high pressure conditions. However, these results require validation using strain gauge measurements. For the validation, the test setup was discussed and four locations for strain gauges was identified. These locations are: M3 multibeam support structure, area between flange and lateral hull, middle rod, and aft area. However, the structural analysis did not contain fatigue life analysis. The central part is made by casting, causing defects that can cause failure of the hull. Fatigue analysis should be conducted in the future.

ACKNOWLEDGMENT

This paper is based on the UNEXMIN project, that has received funding from the European Unions Horizon 2020 research and innovation programme under grant agreement No 690008.

REFERENCES

[1] S. Zavari, O. Usenius, T. Salomaa, J. Villa, A. Heininen, J. Laitinen, J. Aaltonen, and K. T. Koskinen. "Mechatronic Architecture Development of UX-1." Ł (2017): 460-464.

[2] S. Zavari, A. Heininen, J. Aaltonen, and K. T. Koskinen. "Early stage design of a spherical underwater robotic vehicle." In System Theory, Control and Computing (ICSTCC), 2016 20th International Conference on, pp. 240-244. IEEE, 2016

[3] L. Lopes, N. Zajzon, B. Bodo, S. Henley, G. Zibret, and T. Dizdarevic. "UNEXMIN: developing an autonomous underwater explorer for flooded mines." Energy Procedia 125 (2017): 41-49.

[4] D. Sytnyk, R. Pereira, D. Pedrosa, J. Rodrigues, A. Martins, A. Dias, J. Almeida, and E. Silva. "Simulation environment for underground flooded mines robotic exploration." In OCEANS 2017-Aberdeen, pp. 1-6. IEEE, 2017.

[5] J. Yuh. "Design and control of autonomous underwater robots: A survey." Autonomous Robots 8, no. 1 (2000): 7-24.

[6] S. K. Choi, G. Y. Takashige, and J. Yuh. "Experimental study on an underwater robotic vehicle: ODIN." In Autonomous Underwater Vehicle Technology, 1994. AUV'94., Proceedings of the 1994 Symposium on, pp. 79-84. IEEE, 1994.

[7] Y. Chunfeng, S. Guo, M. Li, Y. Li, H. Hirata, and H.Ishihara. "Mechatronic system and experiments of a spherical underwater robot: SUR-II." Journal of Intelligent and Robotic Systems 80, no. 2 (2015): 325-340.

[8] G. Shuoxin, and S. Guo. "Performance Evaluation of a Novel Propulsion System for the Spherical Underwater Robot (SURIII)." Applied Sciences 7, no. 11 (2017): 1196.

[9] Y. Li, S. Guo, and Y. Wang. "Design and Characteristics Evaluation of a Novel Spherical Underwater Robot." Robotics and Autonomous Systems 94, (2017): 61-74.

[10] J. Lianchao, Z. Hu, L. Geng, Y. Yang, and C. Wang. "The Concept Design of a Mobile Amphibious Spherical Robot for Underwater Operation."IEEE, 2016. doi:10.1109/CYBER.2016.7574860.

[11] Y. Li, M. Yang, H. Sun, Z. Liu, and Y. Zhang. "A Novel Amphibious Spherical Robot Equipped with Flywheel, Pendulum, and Propeller." Journal of Intelligent & Robotic Systems 89, no. 3 (2018): 485-501.

[12] A. E. Ibrahim, M. N. Karsiti, and I. Elamvazuthi. "Experimental Depth Positioning Control for a Spherical Underwater Robot Vehicle (URV)." Applied Mechanics and Materials 785, no. Recent Trends in Power Engineering (2015): 729-733.

[13] Zienkiewicz, Olgierd Cecil, Robert Leroy Taylor, Olgierd Cecil Zienkiewicz, and Robert Lee Taylor. The finite element method. Vol. 1. London: McGraw-hill, 1977.

[14] B. Skallerud, T. Iveland, and G. Hrkegrd. "Fatigue life assessment of aluminum alloys with casting defects." Engineering Fracture Mechanics 44, no. 6 (1993): 857-874.

[15] A. L. Window, Strain gauge technology. Springer, 1992.